J Mater Sci (2007) 42:3661–3669
DOI 10.1007/s10853-006-1343-6

Temperature and dwell time effect on hardness of Al-base alloys

F. Abd El-Salam · L. A. Wahab · R. H. Nada · H. Y. Zahran

Received: 26 May 2005 / Accepted: 6 March 2006 / Published online: 30 January 2007

Abstract The hardness of Al–5wt%Zn (alloy A) and Al–5wt%Zn–0.25wt%In (alloy B) was measured at room temperature for samples heat treated in the range 300–453 K and dwell times in the range 30–300 s under 50 gm load. Softening was observed for all the samples and the hardness decreased with increasing temperature and/or dwell time. Hardness drop was larger for alloy (B), which in general showed higher hardness than alloy (A). The stress exponent n increased with increasing temperature and showed high values falling in the power law breakdown region. The parameters deduced from the analysis of X-rays data and micrographs were found to be consistant with the calculated mechanical data.

Introduction

The increasing demand for materials to withstand higher temperatures needs a rapid, inexpensive, non-destructively in situ, method for evaluating the integrity of metallic stuctures [1] and measuring mechanical properties at elevated temperatures [2, 3]. In this regard, hardness H as a complex property related to the strength of interatomic forces and defined as the resistance of a material to local plastic deformation, becomes a handy tool since its measurement can be related in several alloy systems to yield stress σ_y, where typically $H = 3\sigma_y$ in bulk materials [4] as well as to other mechanical properties.

Some complications arise in interpreting hardness values in hard materials such as indentation-induced cracking phenomena, which makes it difficult to measure indent dimensions precisely.

The most important and intractable problem associated with Vickers hardness testing is that concerned with the apparent change in hardness value with change in indentation size, namely, the indentation size effect [5].

Since the hardness test consists of pressing a hard indenter into the surface, it is equivalent to performing a highly localized compression test. As mechanical forming operations are facilitated at high temperature, it can be anticipated that the hot hardness will be lower than that at ambient temperature. It is these hot hardness values that are important in applications such as machining.

The temperature dependence of hardness (H) for metals and alloys is best represented by a relation first suggested by Ito [6] and Shishokin [7] and has been explored by a number of investigators [8, 9].

A functional relationship between hardness H and temperature (T) has been reported [10] as:

$$H = H_0 \exp(-\alpha T) \tag{1}$$

where H_0 is the hardness at zero K, or the intrinsic hardness, and α is the softening coefficient [2, 11] or the coefficient of thermal expansion [8].

F. Abd El-Salam · R. H. Nada (✉) · H. Y. Zahran
Physics Department, Faculty of Education, Ain Shams University, Cairo, Egypt
e-mail: radwanhnada@Yahoo.com

L. A. Wahab
National Centre for Radiation Research and Technology, Nasr-City, Cairo, Egypt

It was reported [8] that hardness decreases with indentation time, following a function of the form [9],

$$H = H_1 t^{-K} \quad (2)$$

where H_1 is the hardness at a given reference time $t = 1$ and K is the so-called creep constant.

One of the useful applications of hardness testing is the prediction of the creep properties of a material [12, 13] and collecting all the creep information from the same sample [3] which can provide incentives in quality control and quality assurance as for reactor core components [14].

In indentation creep test, the indenter is maintained at a constant load over a period of time under well-controlled conditions. As the stresses cause the material beneath the indenter to creep, the indentor penetrates and changes in the indentation size are monitored [2].

Thus the indentation creep test is a prolonged hardness test [15]. It is defined as the time dependent motion of a hard indenter into a solid under constant load [2, 16]. Creep of a number of materials was studied using indentation technique [15, 17, 18].

Indentation creep or impression creep techniques are non-destructive [2] and have several advantages such as small specimen size, ease of specimen preparation, absence of tertiary stage [15], and reduction of the sample for sample variation in property [3]. This enables studying newer and advanced materials in the development stage.

Improvement and optimizing the mechanical properties has been achieved by the addition of alloying elements to binary alloys [19, 20]. The alloys showed various types of creep behaviour, which depend on conditions such as stress, temperature, grain size, and alloy composition [2].

The present work is concerned with the effect of temperature and indium addition on the hardness and indentation creep behaviour of Al–5wt%Zn alloy.

Experimental procedure

The nominal composition of the alloys used in this study was Al–5wt%Zn and Al–5wt%Zn–0.25wt%In. The samples were prepared from high purity elements. The binary alloy will be considered here as alloy A and the tertiary alloy will be taken as alloy B.

Samples of dimensions 10×10 mm were cut from the alloy and metallographically prepared. The samples were heated at 500 °C (773 K) for 2 h, then quenched to room temperature to have the solid solution structure, after which they were heat treated for 3 h at temperatures ranging from 300 K to 453 K followed by quenching to room temperature to retain the structure formed at these annealing temperatures. Micrographs were obtained for these solid solution samples after heat treatment for 3 h at different temperatures around the transformation temperature. All hardness measurements were taken at room temperature by using a Shimadzu 2 series microhardness tester. Indentations were done in the central region of the sample such that they lie away from the edges. Care was taken to maintain the sample surface perpendicular to microscope axis. At each temperature, the average of at least four indentations was reported. The hardness values (H) were measured using a Vickers indenter at 50 gm load (L) on the basis of the standard formula given as [8],

$$H = 1.854\, L/l^2 \quad (3)$$

where l is the diagonal of the residual indentation.

The dwell time of indentation was varied in the range from 30 to 300 s. For each hold time hardness was measured at different temperatures from 300–453 K and a plot was made for hardness (H) versus hold time (t) at each temperature to get the indentation creep measurements.

Results and discussion

The temperature dependence of hardness H and relative hardness H_T/H_{300}, where H_T is the hardness at temperature T and H_{300} is the hardness at room temperature, at 50 gm load and dwell time 60 s for both alloys A & B is given in Fig. 1 which shows that alloy B exhibits higher hardness than alloy A.

Strength of the binary alloy increases with alloying addition where the third element interacts with the different entities in the sample and decreases the mobility of dislocations [11].

In general a softening behaviour dominates with increasing temperature. According to the phase diagram of Al–Zn system [21] given in Fig. 2, heating the alloys A, B at 500 °C then quenching to room temperature brings them to a metastable solid solution structure [21]. In this solid solution a number of additional interactions are possible. These are (1) elastic or Cottrel interaction, (2) electrostatic interaction, (3) short and long-range interactions, (4) chemical interaction and Snoek ordering interactions. These interactions play a role in the resistance of an alloy to

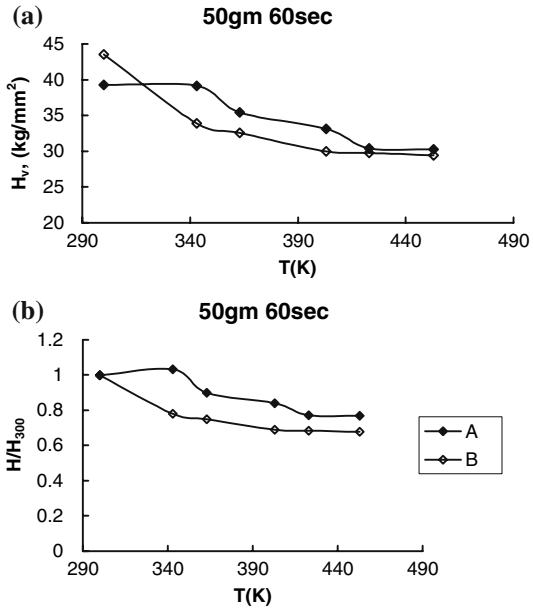

Fig. 1 (**a**) Hot hardness versus temperature for alloy A & B. (**b**) $H_T/H300$ versus temperature for alloy A & B

recovery. The sequence of structure transformation in supersaturated solid solutions of Al–Zn alloys was found [22] to start with the formation of the spherical and the ellipsoidal Guinier Preston zones (GPZ), which are rich in solute atoms, coherent with the matrix, and differ from each other in the thermal stability. The critical temperature for the dissolution of GP zones is assumed not to exceed 225 °C [23]. The transformation of GPZ produces the rhombohedral transition phase (R-phase), which while loosing some coherency yields the Zn-rich FCC ά-phase and finally the Zn rich stable precipitates in the α-matrix. Heating the quenched alloy at temperatures below the line of solubility limit gives rise to controlled precipitation of the second phase with a high level of ductility and fine structure, with average grain diameter of 6.4μm for alloy A at room temperature, Fig. 11a. The dark phase, *β*-phase, dominates within the grains of the bright α-phase. This consists with the statements of the surface activity theory [24] which applies for the two alloys, Figs. 11a and 12a.

In the initial part of the *H–T* curves of Fig. 1, the hardness falls smoothly in the tertiary alloy B but shows a slight increase in the binary alloy A due to the formation of GP zones.

A number of thermally activated dislocation mechanisms have been proposed to account for low temperature yielding [2] of which are slip [2]; deformation twinning [4], breaking away from an interstitial atmosphere; overcoming interstitial precipitates; non-conservative motion of jogs and overcoming Pierls-Nabarro stress which has been widely recognized as the mechanism for softening for the low temperature below 0.25 T_m. In this case the other obstacles, called the athermal obstacles, such as the stress fields of the dislocations, require virtually the entire stress to be applied externally, irrespective of the available thermal energy. As the hardness and flow stress are intimately related [4, 25], the thermal and athermal components of flow stress [2] can be given as [26]:

$$H = H^*(T, \gamma^*) + H_G \tag{4}$$

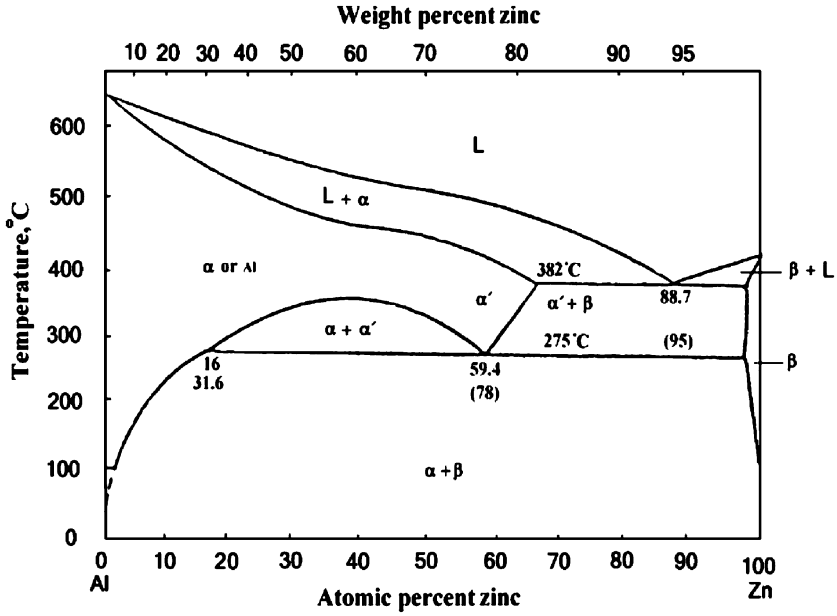

Fig. 2 Phase diagram of Al–Zn system

where, H^* represents the thermal component of hardness which depends on temperature T, γ^* the strain rate and H_G is the athermal component, which is dependent on temperature through the temperature dependance of the shear modulus G. It can therefore be concluded that there exists an athermal part of hardness variation in the obtained hardness values of Fig. 1. This was found previously [2] where the slope of the H–T plot in such region has decreased after correction for the modulus.

For alloy B the migration of the existing lattice defects; vacancies retained in the sample due to quenching, towards their sinks seems to assist the motion of the dispersed Zn (β-phase) and In atoms which cause softening as clear from the initial drop of its H–T curve.

The formation of GP zones and subsequently the formation of β-phase precipitates besides the formation of dislocation loops of vacancy type that may have formed from the retained quenched-in defects and the high induced dislocation density [27] might be the cause of the initial increase in hardness of the binary alloy (A).

Increasing temperature, the hardness increase is followed by a decrease in hardness. This decrease may be attributed to the increased dislocation activity [2] in this region (363–403 K) where GP zones partially dissolve at 343 k, Figs. 11b and 12b, and completely dissolve at 363 k, Figs. 11c and 12c. Also phase transformation takes place yielding grains of 7 μm and then a growth for the second phase precipitates takes place in the two alloys, Figs. 11b and 12b. The dissolution and/or growth of the second phase precipitates take place thus, facilitating dislocation motion between the large and less number of precipitates. The slope of the H–T curve changes suggesting a decrease in the softening rate due to the operation of some additional mechanisms. It may be that the softening due to additional slip systems is counterbalanced by the occurrence of dynamic strain aging process, which may lead to athermal region in the H–T curve, Fig. 1.

At higher temperatures, 423–453 K, where the β-phase becomes highly dispersed forming a solid solution with grains of 8.86 μm, Figs. 11d and 12d, the hardness falls to a level depending on the deformation conditions. The mechanisms proposed [28] for softening in this temperature range are diffusion—controlled phenomena, such as dislocation climb and glide processes. The average grain diameters obtained for alloy A due to different annealing temperatures are given in Table 1.

Table 1 The average grain diameters obtained for alloy A due to different annealing temperatures

Annealing temperature k	Average grain diameter μm
300	6.4
343	7.89
363	7.0
423	8.86

Applying Eq. (1), Fig. 3a, yields for the binary alloy (A)

$$\ln H = -0.0019\ T + 4.2894 \tag{5}$$

and Fig. 3b gives for the tertiary alloy (B):

$$\ln H = -0.0027T + 4.5713 \tag{6}$$

It is clear that the softening coefficient α is higher for the alloy (B) (0.0027), than that of the In free alloy (A) (0.0019). This consists with the drop in hardness obtained from Fig. 1, which reaches 67.7% of its room temperature value for alloy (B), while it falls only to 77% for the In free alloy (A). Also, the increased hardness of alloy B due to the presence of In still exists at all temperatures even at 0 K where the intrinsic hardness of alloy (B), 96.67, is larger than that of the In free alloy (A), 72.92, as obtained from Eqs. 5, 6, respectively.

The difference in the composition of the two alloys makes alloy (B) an off-stoichiometry alloy and

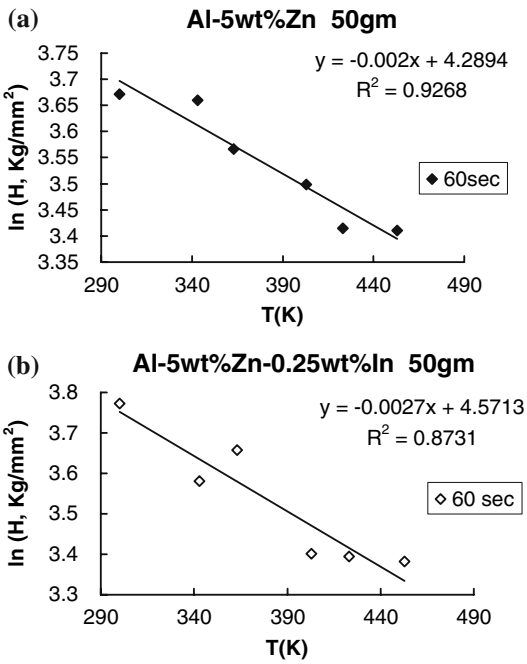

Fig. 3 LnH versus temperature for (**a**) alloy A, (**b**) for alloy B

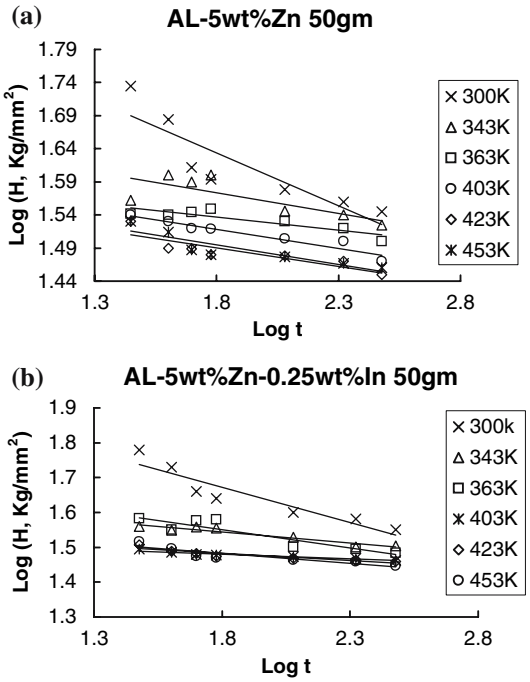

Fig. 4 Log H versus log t at a constant load 50 gm, and different temperatures (**a**) for alloy A, (**b**) for alloy B

additional strengthening from constitutional defects may help retain the hardness all over the tested temperature range.

Indentation creep experiments were carried out on both alloys A, B over the same temperature range, 300–453 K, using a load of 50 gm.

The hardness versus time data obtained from indentation creep experiments was ploted in a log–log plot for different temperatures as shown in Fig. 4a for alloy (A), and Fig. 4b for alloy (B). There is clear time dependence of hardness at any temperature for both alloys.

In an elastic–plastic analysis of the hardness test, when an indenter is pressed into the flat surface of the solid, the indenter is encased in a non-deforming core within which there is assumed to be a hydrostatic pressure. Outside this zone, there exists a plastic-elastic zone surrounding the hydrostatic zone. The process of indentation is thus linked to be the plastic movement of a series of shells concentric with the core into the bulk of the specimen [2]. Therefore, Sargent and Ashby's model [29], based on dimensional analysis, was adopted here to analyse the obtained time dependent hardness data. The observed hardness decrease with dwell time, Fig. 4 as a common phenomenon [8] is indicative of the material undergoing creep deformation. The equation derived for this model is given by:

Table 2 Stress exponent (n) for alloys A and B at 50 gm load and different temperatures

Temperature (K)	The value of n for alloy A	The value of n for alloy B
300	6.28	4.89
343	16	15.5
363	25.3	9.47
403	17.4	37
423	17.8	24.4
453	16.9	17.7

$$H(t) = (\sigma_0) / (nc\varepsilon_0 t)^{1/n} \quad (7)$$

where $H(t)$ is the time dependent hardness, $\acute{\varepsilon}_o$ is the strain rate at reference stress σ_o, c is a constant and n is the stress exponent. From the above equation, the slope of the log H versus log time plot at constant temperature is $-1/n$. The values of n for alloys A and B as calculated at 50 gm load from Fig. 4a, b are given in Table 2.

The values of n for both alloys increased with temperature to high values. At room temperature (300 K) the value 6.28 for alloy A consists with dislocation glide as diffusion controlled process [11]. For alloy B, the value 4.89 falls in the climb regime for which n is generally taken to be about 5 [30].

For values of n in the range 20–33 in Table 2 the probable mechanism is dislocation interaction [11].

In the elastic–plastic zone of indentation, the stress can be fairly high especially at low homologous temperatures. So, to account for high n values obtained in Table 2, it was shown [29] that the hardness data associated with such low temperatures and high stresses may fall in the power law breakdown region where the creep rate and stress are expected to obey exponential relation. In view of this state, as a value of 37 is obtained in this work for alloy (B), in another indentation creep studies a value of $n = 60$ was obtained for Cu and a value around 20 was reported for Si [15].

The temperature dependence of n values given in Table 2, is given in Fig. 5a, b for both alloys (A) and (B), respectively.

According to Eq. (2), the values of hardness H_1 at a given reference time = 1 and the creep constant k are given in Table 3 for alloys (A) and (B) at different temperatures under 50 gm load.

The data in Table 3 show a general decrease of the hardness values H_1 with increasing temperature, which consists, with the decreasing behaviour of hardness with increasing temperature. The values of H_1 also point to the effect of (In) which increases the hardness

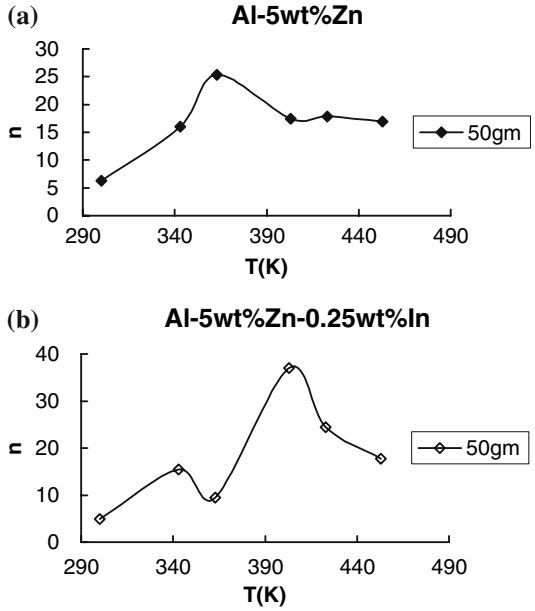

Fig. 5 Stress exponent (n) versus temperature at load 50 gm (**a**) for alloy A, (**b**) for alloy B

Table 3 H_1 at time one second and creep constant k for alloys A and B at 50 gm load and different temperatures

Temperature (K)	H_1 (Kg/mm^2) for alloy A	H_1 (Kg/mm^2) For alloy B	K for alloy A	K for alloy B
300	83.72	110.69	–0.160	–0.207
343	45.03	45.88	–0.049	–0.067
363	28.85	40.77	–0.029	–0.052
403	45.36	33.81	–0.076	–0.027
423	40.92	35.73	–0.065	–0.040
453	40.02	38.29	–0.060	–0.056

of alloy B ($H_1 = 110.69$) over that of alloy A ($H_1 = 83.72$) at room temperature and supports the values of hardness drop which was found to be greater for alloy B (67.7%) than that of alloy A (77%) obtained from Fig. 1.

The variations of the time exponent or the so-called creep constant show the same behaviour in both alloys A and B.

At low temperatures, the value of K is relatively high implying higher times for creep to proceed in a matrix with hindering intities of the GP zones and other second phase precipitates.

The effect of (In) is still existing as reflected in Table 3 by the higher value ($K = 0.207$) for alloy B than that ($K = 0.160$) value for alloy A. Increasing temperature, the matrix components formed tend to dissolve near the transformation temperature leading to softening which assists creep and lowers the time exponent K. After transformation, according to the phase diagram [21] of Fig. 2, solid solution hardening shows itself as another increase in the time exponent K of Eq. 2. It is clear that (In) may have caused retardation in transformation since K increased at 403 K for alloy (A) but at 423 K for alloy (B).

Hardening due to indium still affects the state of alloy (B) as clear from the continuous increase of K value while it has a decreasing behaviour above the transformation temperature of the (In) free alloy (A). Finally, at the higher temperature 453 K the components in the matrix of alloy (A) seem to have more order than those of alloy (B) and therefore some slight henderence increase is retained for alloy (A) over that of alloy (B).

Finding the time required to attain a constant hardness at different temperatures, the apparent activation energy of creep has been computed from plots of Fig. 6 relating log t vs. log $(1/RT)$ at constant hardness value. The values 206 and 411 kJ/mol obtained for alloy (A) and alloy (B), respectively consist with the mechanisms related to the stress exponent values mentioned here before.

The activation volume, which denotes the volume over which the thermal energy is to concentrate in order to achieve the activation, is defined as [15]:

$$V^* = KT\,(\Delta \ln \dot{\varepsilon}/\Delta\sigma) \tag{8}$$

where K is Boltzmann's constant. To evaluate the deformation partial, $\Delta \ln \dot{\varepsilon}/\Delta\sigma$, Atkin's model [31] is employed to generate the creep curves with the strain identified with $H^{-1.5}$ and is therefore in arbitrary units [15]. For the obtained creep curves given in Fig. 7a, b (for alloy (A) and alloy (B), respectively), in most

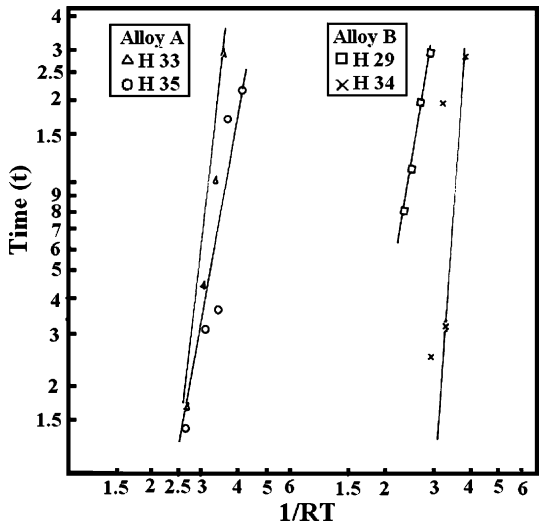

Fig. 6 Log time versus log $1/RT$ at load 50 gm and different values of hardness for alloys A & B

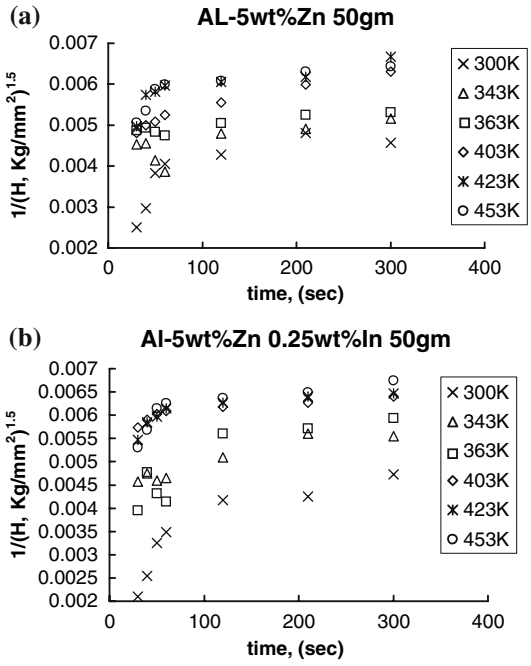

Fig. 7 $1/H^{1.5}$ versus time at load 50 gm and different temperatures (**a**) for alloy A, (**b**) for alloy B

cases a nearly steady state seems to be attained after 120 s. From Fig. 7, at constant temperature, the creep rate $\acute{\varepsilon}$ is obtained. As the hardness is known, the corresponding stress can be computed and the quantity $\Delta \ln \acute{\varepsilon}/\Delta\sigma$ is then calculated from Fig. 8a, b and substituted in Eq. (8) to yield the magnitude of the activation volume, whose temperature dependence is given in Fig. 9 for both alloys A, B. It is observed that, in

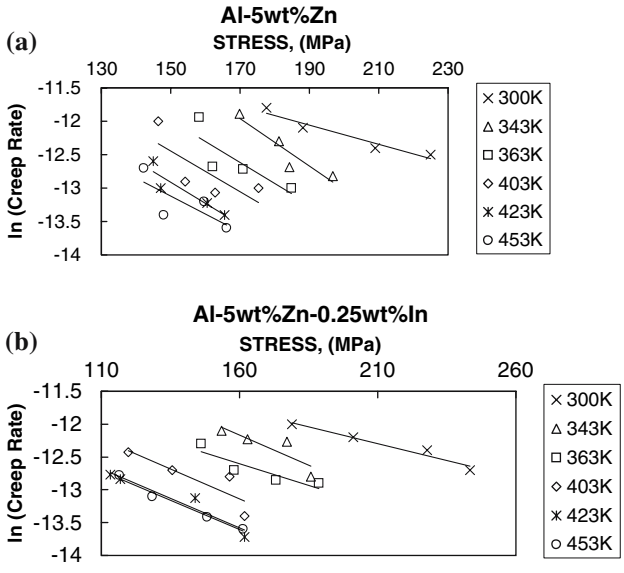

Fig. 8 ln creep rate versus stress (Mpa) at different temperatures (**a**) for alloy A, (**b**) for alloy B

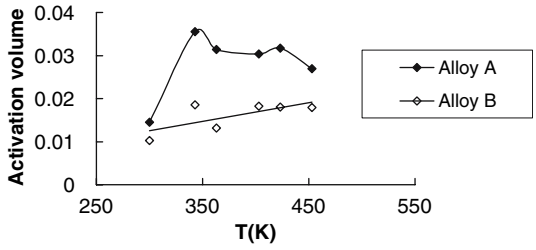

Fig. 9 Activation volume versus temperature for alloys A & B

general, the activation volume increases with increasing temperature, which can be explained in terms of the dislocation density, ρ.

The activation volume is proportional to the average spacing of dislocations [32]. As the thermal energy is provided, the dislocation density decreases and the average distance between dislocations increases, leading to the increase of the activation volume with increasing temperature. The activation volume reveals the integrated role between temperature and stress for facilitating the dislocations overcoming both the thermal and athermal obstacles and increasing the strain rate.

X-ray diffraction patterns were obtained at room temperature for samples following the same procedure for hardness testing at the different temperatures. On the assumption that the particle size, (η), and the macrostrain (ε) obey a Cauchy distribution [33]; the following equation

$$B\cos\theta/\lambda = 1/\eta + 2\varepsilon \sin\theta/\lambda \quad (9)$$

with θ, the peak angle and λ the wavelength of the used X-ray, can be used to analyze the obtained X-ray diffraction patterns. From the straight lines relating $B\cos\theta/\lambda$ and $\sin\theta/\lambda$ at different temperatures, a half of the slope refers to the lattice strain ε, and the inverse of the intercept on the ordinates gives the average crystallite size η. The average internal strain ε_{av} and the average crystallite size η_{av} for the different working temperatures are given in Fig. 10a, b, respectively. The dislocation density ρ is related [34] to $1/\eta^2$, and its temperature dependence is shown in Fig. 10c.

It is clear that small crystallite size is due to large lattice strain and high dislocation density. The quenched state (300 K) has small grains and increasing temperature increases grain size due to thermal strain recovery and a decrease of dislocation density. The fluctuations in the values of the crystallite size of Fig. 10 which consist with the values obtained from the micrographs of Fig. 11 and shown in Table 1, and the corresponding inverse variations of lattice strain and

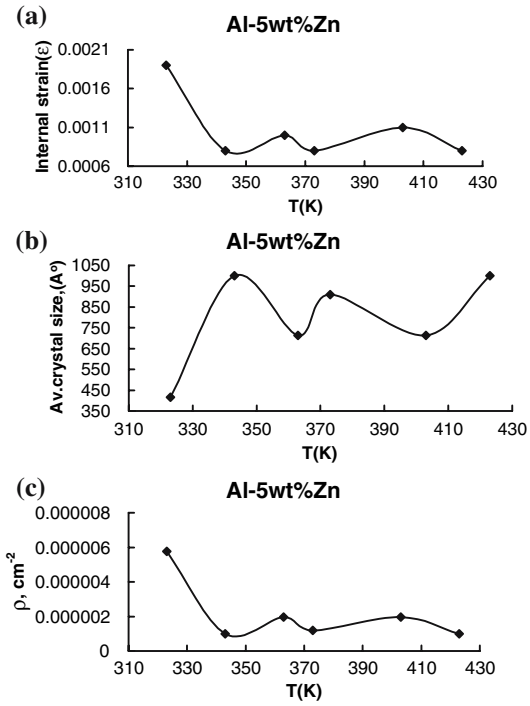

Fig. 10 (**a**) Internal strain (ε) versus temperature for alloy A, (**b**) Average crystal size η_{av} (A°) versus temperature for alloy A, (**c**) Density of dislocations ρ (cm^{-2}) versus temperature for alloy A

dislocation density depend mainly on the thermal and athermal variations in the different structural components of the alloy. The behaviour of variation in the parameters of Fig. 10, agrees well with the softening behaviour observed in Fig. 1. The parameters in Fig. 10a, c deduced from X-ray data confirm the behaviour of the activation volume of Fig. 9, deduced from creep measurements.

Conclusion

Al–5wt%Zn (alloy A) and Al–5wt%Zn–0.25wt%In (alloy B) were heated at 500 °C for 2 h then quenched in water to room temperature to have the solid solution structure.

Samples of the two alloys were heated in the temperature range 300–453 K for 3 h then quenched in water to retain the structure formed at the annealing temperature.

Vickers hardness measurements were carried out at room temperature under 50 gm load and dwell times ranging from 30 to 300 s.

Hardness was found to decrease with increasing temperature and/or dwell time. Indium increased the hardness for all the tested temperatures. The stress exponent n changed for both alloys at different temperatures pointing to diffusion controlled processes and the high values were considered to fall in the power law breakdown region.

Indentation creep data gave average activation energies of 206 and 411 kJ/mol for alloys A and B, respectively. The values obtained for the activation volume increased with increasing temperature. The

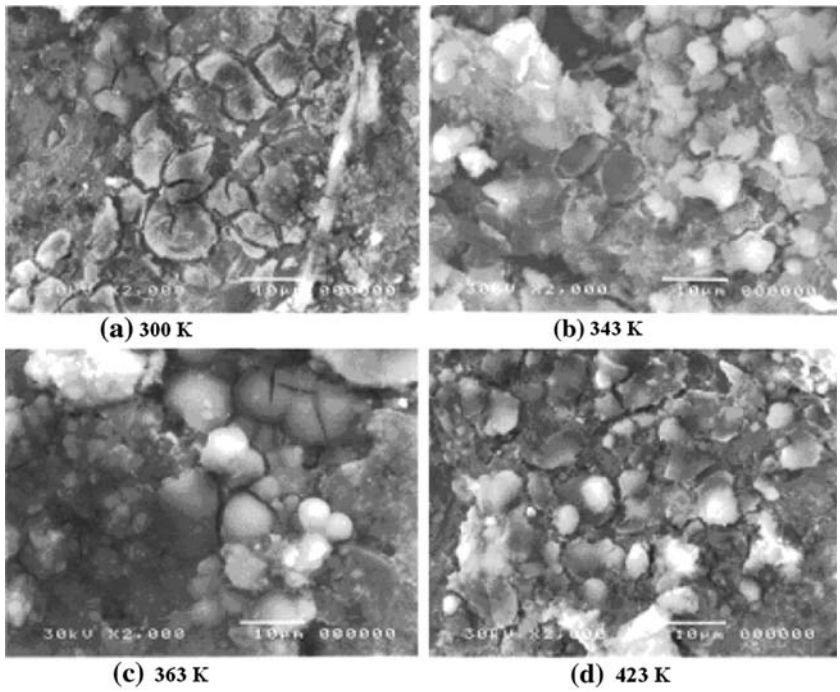

Fig. 11 Micrographs for samples of alloy A solution treated then heated for 3 h at different temperatures

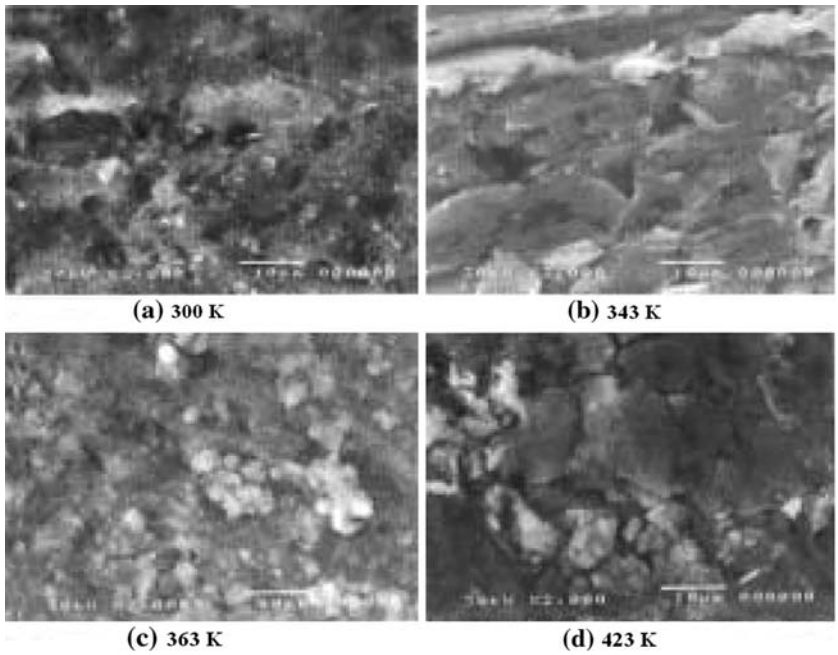

Fig. 12 Micrographs for samples of alloy B solution treated then heated for 3 h at different temperatures

behaviour of the temperature dependence of the parameters calculated from X-ray data were found to agree with that from the micrographs and the mechanical results.

References

1. Haggag FM, Nanstad RK, Braki DN (1989) Amer Soc Mech Eng, Book No. H00485 pvp-vol.170:101
2. Sharma G, Ramanujan RV, Kutty TRG, Tiwari GP (2000) Mater Sci Eng A 278:106
3. Chiang D, Li JCM, (1994) J Metal Res 9:903
4. Petty ER, O'neill H (1961) Metallurgia 63:25
5. Cal X, Yang X, Zhou P (1997) J Mater Sci Lett 16:741
6. Ito K (1923) Sci Rep Tohoku Imp Univ. 112:137
7. Shishokin VP, Anorg Z (1930) Chem 189:263
8. BatlaCalleja FJ, Flores A, Ania F, Bassett DC (2000) J Mater Sci 35:1315
9. BatlaCalleja FJ (1985) Trends Polym Sci 66:117
10. Kramer BM, Judd PK (1985) J Vac Sci Tech A3 6:2439
11. Kutty TRG, Jarvis T, Ganguly C (1997) J Nucl Mater 246:189
12. Westbrook JH (1953) Trans Am Soc Met 45:221
13. Geach GA (1974) Int Met Rev 19:255
14. Rodriguez P (1991) In: Proc on Zirconium alloys for reactor components (ZARC-91), Department of Atomic Energy, Bombay, p 46
15. Sundar RS, Kutty TRG, Sastry DH (2000) Intermetallics 8:427
16. Li WB, Warren R (1993) Acta Metall Mater 41:3065
17. Chu SNG, Li JCM (1977) J Mater Sci 12:2200
18. Kutty TRG, Ganguly CG, Sastry DH (1996) Scripta Metall Mater 34(12):1833
19. Mckamey CG, Devan JH, Tortorelli PF, Sikka VK (1991) J Mater Res 6:1779
20. Sikka VK (1991) Ductility enhancement of iron aluminide alloy, SAMPE Q 7:2
21. Hansen M, Anderko K (1958) Constitution of binary alloys. MC Grow-Hill, New York, p 149
22. Mostafa MM, Nada RH, Abd El-salam F (1994) Phys Stat Sol A 143:297
23. Abd El-Salam F, Ibraheim AM, Ammar AH, Morsy AY (1995) Vacuum 46(11):1299
24. Semenchenko VK (1961) Surface phenomena in metals and alloys. Pergamon, London
25. Atkins AG, Tabor D (1966) Proc R Soc London Ser A 292:441
26. Stone DS, Yoder KB (1994) J Mater Res 9:2524
27. Krishnamurthy S, Gupta SP (1977) Mater Sci Eng 3:155
28. Westbrook JH (1956) J Electrochem Soc103:54
29. Sargent PM, Ashby MF (1992) Mater Sci Tech 8:594
30. Linga Murty K, Ravi J, Wiratmo (1995) Nuc Eng Des 156:359
31. Atkin G (1971) In: Westbrook JH, Conrad H (eds) The science of hardness testing and its research applications. A.S.M, Metals park (OH), p 223
32. Garofalo F, (1965) Fundamentals of creep and creep rupture in metals. New York and London, p 29
33. Warren BE (1959) Rep Prog Metals 8:47
34. Fawzy A, Mostafa MT, Abd El-Salam F (2001) Egypt J Sol 24(1):79